IEEE Open Journal of
Power Electronics

Received 25 April 2022; accepted 13 May 2022. Date of publication 23 May 2022;
date of current version 2 June 2022. The review of this article was arranged by Associate Editor Prof. H. Alan Mantooth.

Digital Object Identifier 10.1109/OJPEL.2022.3176833

Model Predictive Control of Non-Isolated DC/DC Modular Multilevel Converter Improving the Dynamic Response

RAMIN RAZANI AND YASSER ABDEL-RADY I. MOHAMED (Fellow, IEEE)

University of Alberta, Edmonton, AB T6G 2R3, Canada

CORRESPONDING AUTHOR: RAMIN RAZANI (e-mail: razani@ualberta.ca)

This research was supported by funding from the Canada First Research Excellence Fund as part of the University of Alberta's Future Energy Systems research initiative, and Alberta Innovates Graduate Student Scholarship.

ABSTRACT The model predictive control (MPC) is a well-accepted method for controlling power electronic converters. This paper presents a tailored MPC approach in which the internal and external dynamics of the dc/dc modular multilevel converter (MMC) are integrated into the MPC algorithm. The proposed MPC approach introduces three control objectives to have full control over the internal and external dynamics. Each of the designed cost functions includes one primary term regulating one of the control objectives and one secondary term improving the converter performance. Unlike the conventional control approach based on multiple proportional-integral (PI) controllers, the proposed approach provides a straightforward way to design the control parameters. The operation of the presented MPC approach is thoroughly investigated and compared to that of the PI-based controller. Comparative simulation studies confirmed that the proposed MPC approach reduces the ac circulating current in the steady-state operation compared to the conventional PI-based control. In the transient mode, the MPC approach offers much smoother and faster responses to the changes in the power reference. The performance of the dc/dc MMC controlled by the proposed MPC approach under parametric uncertainty is investigated, and improved performance is obtained compared to the conventional PI-based control.

INDEX TERMS DC/DC Modular Multilevel Converter (MMC), Model Predictive Control (MPC), Computational burden, Improved Dynamic response.

I. INTRODUCTION

Nowadays, renewable energy sources have gained escalating importance due to environmental and economic reasons. As one of the drawbacks, they are mostly located in distant regions. Hence, the generated energy has a long path to reach consumers [1]. The High-Voltage dc (HVdc) and Medium-Voltage dc (MVdc) systems have been proposed in the last decades to answer this need. Because of the superiority of these systems over the old-school ac systems, they are being established all over the world. Recently, researchers have proposed the idea of dc grids which can be realized by connecting the existing dc systems. This notion can improve the efficiency and stability of the power system [2]. One of the most concerning challenges related to this idea is that the existing dc systems are built through time. Hence, they are possibly built with different nominal voltages and grounding structures, making their interconnection even more challenging. To tackle this challenge, various topologies of high-voltage and high-power dc/dc converters are suggested in the literature [3].

To have the advantages of the well-known dc/ac modular multilevel converter (MMC) [3]–[5], researchers developed different dc/dc converters based on the dc/ac MMC topology. In [6], the modular multilevel dual-active-bridge (DAB) was proposed; it consists of two full-scale dc/ac MMCs connected via a medium-frequency transformer. As the Modular Multilevel DAB requires two fully rated MMCs, the overall size and the cost of the system are significant. The idea of non-isolated dc/dc MMC was presented in [7] and [8]. The non-isolated dc/dc MMC proposed in [8] requires extra submodule (SMs) and additional current paths to prevent the harmonic contents

from reaching the dc-links. While the non-isolated dc/dc MMC developed in [7] only requires inductive filters to eliminate the harmonic contents. This topology has the simplest structure, the smallest number of SMs, and the highest efficiency among the MMC-based dc/dc converters. Hence the non-isolated dc/dc MMC with passive filters developed by [7] is selected as the focus of this study, and from now on, it is simply called the dc/dc MMC.

In the recent studies, design [9], [10], and modeling [11]–[13] aspects of the dc/dc MMC were studied. The capacitors voltages of the hybrid dc/dc MMC were investigated in [14], which was shown that the capacitors voltages could not be kept balanced when the transferred power exceeds a certain value limiting the converter operation. The operation of the dc/dc MMC in the presence of SM fault was studied in [15]. This article uses the dc/dc MMC features to enable fault-tolerant operation without adding additional SMs. The control aspect of the dc/dc MMC is studied in [16]–[19]. In [16], a capacitor voltage balancing strategy that reduces the circulating current was proposed. The operation principle of the hybrid dc/dc MMC was explained in [17], where the power transfer capability is improved by utilizing the elevated capacitors voltages. In [18], the full-state regulation of the dc/dc MMC was proposed to minimize the ac circulating current. Authors in [19] introduced a new closed-loop control of the dc/dc MMC to ensure energy balancing in the load transient and steady-state. To date, all the suggested control approaches are based on proportional-integral (PI) controllers. This type of controller suffers from the complexity of handling multiple control objectives and poor transient performance. As the number of control objectives grows, the number of needed PI loops increases resulting in the complexity of the overall control structure and the difficulty of PI parameters tuning.

In the previous literature, to overcome the disadvantages of the PI-based controllers, researchers widely used the model predictive control (MPC) for the control of the dc/ac MMC [20]–[25]. In [20], the computational burden of the MPC was reduced by decoupling the capacitors voltage balancing from the MPC algorithm. This task was realized in a separate sorting algorithm. By solving the Diophantine equations, the online optimization and presence of the weighting factors were avoided in [21], which resulted in a lower computational burden and enhanced reliability. Authors in [26] used MPC to detect the fault and enable the operation of the converter after the fault. This approach can locate the faulty SM within one fundamental period. A new modulated MPC for the dc/ac MMC was proposed in [24], where it used two predetermined voltage levels to build the voltage reference. To improve the computational burden and the steady-state performance of the converter and eliminate the need for weighting factors, a new MPC approach called the sliding-discrete control set was introduced in [25]. To date, a few studies [27], [28] developed MPC methods for the isolated dc/dc MMC. In general, this topology is built of two dc/ac MMCs which are connected via an ac transformer. In [27], a modulated MPC approach was proposed for the inductor-less MVDC MMC, which reduces the computational burden by reformulating the underlying optimization problem. The author in [28] proposed a Finite Control Set MPC to regulate the output voltage. This is achieved by defining a cost function, including the output voltage, which yields the optimum number of SMs in the next control period.

Despite extensive studies on the application of the MPC method in the control of the MMC-based converters, to date, the MPC method has never been used for the control of the dc/dc MMC introduced in [7]. Although these converters, the dc/dc and the other MMC-based converters, share a similar topology, there exist crucial differences in the operation principle. Moreover, the control objectives and the control variables of these two converters are totally different. Therefore, the developed MPC methods for the other MMC-based converters cannot be used directly for the dc/dc MMC. This paper develops a tailored MPC approach for the control of the dc/dc MMC. First, the internal and external dynamic equations of the converter are extracted. Then, a new set of variables is introduced to decouple the equations, making the control algorithm simpler. Using the Forward Euler method, the decoupled dynamic equations are discretized, forming the discrete-time model of the dc/dc MMC. Three control objectives are introduced to have full control over the converter dynamics. Thanks to the decoupled dynamic equations, each one of the control objectives is regulated by minimizing a separate cost function. The designed cost functions have one primary term regulating one of the control objectives and one secondary term that improves the converter performance. In the end, the proposed MPC is investigated in the load transient and the steady-state, and the obtained results are compared with the conventional PI-based controller. An extensive sensitivity analysis is also carried out to investigate the performance of the dc/dc MMC controlled by the proposed MPC approach under parametric uncertainty.

II. STRUCTURE AND OPERATION PRINCIPLE

A. STRUCTURE

Fig. 1. illustrates a dc/dc MMC with two-phase legs. As shown, each phase-leg is built of two stacks of submodules (SMs) and two arms inductors L. Each stack contains N number of SMs with a nominal voltage of $V_{cn} = \frac{V_{DC2}}{N}$. The SM structure can be chosen from any topology of the voltage source converters, such as half-bridge and full-bridge converters. Since the half-bridge-based SMs (HBSMs) offers the lowest number of components and the highest efficiency, it is used in this paper, as shown in Fig. 1. The HBSM is turned on whenever S_1 is on and S_2 is off, and it is turned off when S_1 is off and S_2 is on (see Fig. 1). The arms inductors are vital for the converter to operate properly. Because they make it possible for every two arms of one phase-leg to exchange ac power. Moreover, they limit the fault current and attenuate harmonic currents in the arms. As exhibited in Fig. 1, a phase inductor L_0 connects the phase legs to the dc-link 1. The phase inductor restrains the circulating current from leaking into

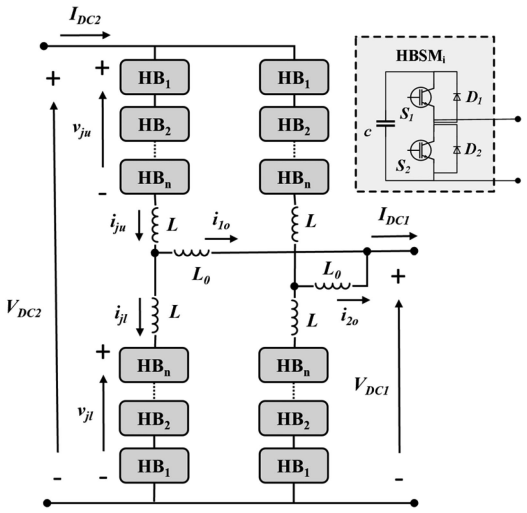

FIGURE 1. Basic structure of a two phase-leg dc/dc MMC and the HBSM.

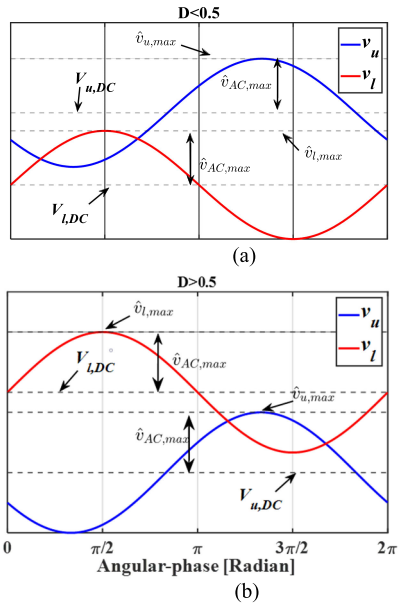

FIGURE 2. The upper and lower arms voltages references in the condition in which the arm ac voltage is set at maximum value, (a) $D < 0.5$, (b) $D > 0.5$.

dc-link 1. From Fig. 1, the dc-link 2 voltage V_{DC2} is higher than the dc-link 1 voltage V_{DC1}. I_{DC1} and I_{DC2} show the dc-links currents. The upper and lower arms voltages generated by the serried SMs are shown by v_{ju} and v_{jl}, respectively. i_{ju} and i_{jl} stand for the upper and lower arms currents. The subscript j indicates the phase-leg, which is under investigation.

B. OPERATION PRINCIPLE

Assuming that the converter transmits P power to the dc-link 1 ($P > 0$), the processed dc power by the arms (upper and lower arms) P_{DC} are equal and calculated by

$$P_{DC} = \frac{1-D}{M} P \tag{1}$$

$$D = \frac{V_{DC1}}{V_{DC2}} \tag{2}$$

where D is the conversion ratio, and M denotes the number of the phase legs. The ac power P_{AC} is interchanged between the arms of one phase-leg to neutralize the dc power flow P_{DC} in each arm. The average absorbed energy by the arm would be zero if P_{AC} equals to -P_{DC} . This condition will guarantee the capacitors voltages balance. To generate P_{AC}, the arms references voltages need an ac part to produce an ac current flowing through the arms. The arms voltages' references v_{ju} and v_{jl} are exhibited in (3) and (4).

$$v_{ju}(t) = (V_{DC2} - V_{DC1}) + \hat{v}_{ju,AC} \cos(2\pi f t + \varphi) \tag{3}$$

$$v_{jl}(t) = V_{DC1} + \hat{v}_{jl,AC} \cos(2\pi f t) \tag{4}$$

In which f exhibits the operating frequency, and $\hat{v}_{u,AC}$ and $\hat{v}_{l,AC}$ show the amplitude of arms ac voltages. φ stands for the phase difference between the arms ac voltages. As can be seen, there exist two components in the arms voltages, dc and ac parts. The dc voltage regulates the dc power, and the ac voltage tunes the active ac power. The operating frequency is a design parameter which, by increasing it, the size of passive components can be decreased at the cost of higher switching losses. To ensure that the induced ac circulating currents in the phase-legs do not leak into dc-links, the ac voltages of phase-legs have $\frac{2\pi}{M}$ phase shift. In this sense, the summation of the ac currents existing in the phase-legs will be zero. The phase-difference φ is an important parameter in the control of dc/dc MMC, since it can regulate P_{AC}. Authors in [16] and [17] stated that to have the minimum circulating current the following conditions should be satisfied: 1) the amplitudes of arms ac voltages of one phase-leg, $\hat{v}_{ju,AC}$ and $\hat{v}_{jl,AC}$, must be equal. 2) the arms ac voltages must be set at the maximum value. Because in this study, these two conditions are satisfied, from now on, $\hat{v}_{ju,AC}$ and $\hat{v}_{jl,AC}$ are denoted by v_{AC}. The maximum arm ac voltage depends on the dc component of arms voltages. Because the arm voltage cannot be a negative value and cannot exceed V_{DC2}, the maximum feasible ac voltage is equal to half of swing range of the arm voltage. To explain it more, Fig. 2 is presented, where the arms voltages in two conditions, $D < 0.5$ and $D > 0.5$, are illustrated. For example, when $D < 0.5$, the upper arm voltage is restricted from above (cannot exceed V_{DC2}) and the lower arm voltage is limited from bottom (cannot be less than 0). In this condition the half of swing range of the upper and the lower arms voltages are $V_{DC2} - v_{u,DC}$ and $v_{l,DC}$, respectively. The maximum ac voltage that can be applied is equal to the minimum of these two values. Having the mentioned limitations in mind and noticing the conditions of minimizing the ac circulating current ($\hat{v}_{ju,AC} = \hat{v}_{jl,AC}$), the maximum ac voltage of one phase-leg at any time instant can be found by

$$v_{AC,max} = min\{v_{u,DC},\ v_{l,DC},\ V_{DC2} - v_{u,DC},\ V_{DC2} - v_{l,DC}\} \tag{5}$$

In which $v_{u,DC}$ and $v_{l,DC}$ denote the dc components of upper and lower arms voltages. In transient mode, they can change to regulate the transferred power. While in the steady-state, $v_{u,DC}$ and $v_{l,DC}$ have a fixed value of $V_{DC2} - V_{DC1}$ and V_{DC1}. Accordingly, the arm ac voltage in steady-state $v_{AC,ss}$ is equal to $V_{DC2} - V_{DC1}$, when $D > 0.5$, and is equal to V_{DC1} when $D < 0.5$.

III. DYNAMIC MODEL

A. CURRENTS AND VOLTAGES

By writing KVL equations in the dc-links 1 and 2 loops and from dc-link 2 to dc-link 1, the following dynamic equations are derived.

$$V_{DC1} - v_l + L_0 \frac{d}{dt}(i_u - i_l) - L \frac{d}{dt} i_l = 0 \quad (6)$$

$$V_{DC2} - v_u - v_l - L \frac{d}{dt}(i_u - i_l) = 0 \quad (7)$$

$$V_{DC2} - V_{DC1} - v_u - L_0 \frac{d}{dt}(i_u - i_l) - L \frac{d}{dt} i_u = 0 \quad (8)$$

As can be seen, in this study, the resistance of the arm and phase inductors is ignored. By subtracting (8) from (6), the following equation is obtained.

$$-V_{DC2} + 2V_{DC1} + v_u - v_l + 2L_{eq} \frac{d}{dt}(i_u - i_l) = 0 \quad (9)$$

In which L_{eq} is defined as $L_0 + \frac{L}{2}$. To have decoupled equations, a new set of variables are defined as:

$$v_{diff} = \frac{v_u + v_l}{2} \quad (10)$$

$$v_s = \frac{v_u - v_l}{2} \quad (11)$$

$$i_{diff} = \frac{i_u + i_l}{2} \quad (12)$$

$$i_s = i_u - i_l \quad (13)$$

In which v_{diff} and v_s show the differential and output voltages, and i_{diff} and i_s are the differential and output currents. By replacing (10)–(13) in (7) and (9), the following equations can be derived.

$$L \frac{di_{diff}}{dt} = \frac{V_{DC2}}{2} - v_{diff} \quad (14)$$

$$L_{eq} \frac{di_s}{dt} = \frac{V_{DC2}}{2} - v_{DC1} - v_s \quad (15)$$

v_{diff}, v_s, i_{diff} and i_s have dc and ac parts just like the arms voltages and currents. To have control over the dc part of i_{diff} and i_s ($i_{diff,dc}$ and $i_{s,dc}$), the dc parts of variables in (14) and (15) can be separated from the ac parts, and these equations can be rewritten by the dc parts as:

$$L \frac{di_{diff,dc}}{dt} = \frac{V_{DC2}}{2} - v_{diff,dc} \quad (16)$$

$$L_{eq} \frac{di_{s,dc}}{dt} = \frac{V_{DC2}}{2} - v_{DC1} - v_{s,dc} \quad (17)$$

Using the Forward Euler equation, (16) and (17) can be discretized as presented in (18) and (19).

$$i_{diff,dc}(t + T_s) = i_{diff,dc}(t) + \frac{T_s}{L}\left(\frac{V_{DC2}}{2} - v_{diff,dc}(t)\right) \quad (18)$$

$$i_{s,dc}(t + T_s) = i_{s,dc}(t) + \frac{T_s}{L_{eq}}\left(\frac{V_{DC2}}{2} - V_{DC1} - v_{s,dc}(t)\right) \quad (19)$$

B. SMS ENERGIES

The stored energies in each arm can be found using (20) and (21).

$$\frac{dW_u}{dt} = v_u . i_u \quad (20)$$

$$\frac{dW_l}{dt} = v_l . i_l \quad (21)$$

Then, by defining sum and differential energies, W^{Σ} and W^{Δ}, in (22) and (23), (20) and (21) can be rewritten as demonstrated in (24) and (25).

$$W^{\Delta} = W_u - W_l \quad (22)$$

$$W^{\Sigma} = W_u + W_l \quad (23)$$

$$\frac{dW^{\Delta}}{dt} = p^{\Delta} = v_{diff} . i_s + 2v_s . i_{diff} \quad (24)$$

$$\frac{dW^{\Sigma}}{dt} = p^{\Sigma} = 2v_{diff} . i_{diff} + v_s . i_s \quad (25)$$

In which p^{Σ} and p^{Δ} are the sum and the differential instantaneous powers of the upper and lower arms. The sum and differential energies include dc and ac components. The ac parts of energies are caused by the capacitors voltages fluctuation around the nominal voltage. However, the dc parts are the control objectives in the dc/dc MMC, and they need to be controlled to ensure the capacitors voltages balance. In this sense, (24) and (25) are required to be rewritten by only dc components. To accomplish this, the ac components of differential and output voltages and currents need to be found. From (3) and (4), the ac component of v_{diff} and v_s is formulated as:

$$v_{diff,ac}(t) = v_{ac} \cos\left(\frac{\varphi}{2}\right) . \cos\left(wt + \frac{\varphi}{2}\right) \quad (26)$$

$$v_{s,ac}(t) = -v_{ac} \sin\left(\frac{\varphi}{2}\right) . \sin\left(wt + \frac{\varphi}{2}\right) \quad (27)$$

Since the control of the sum and the differential energies are not meant to be fast, the ac component of differential and output currents can be calculated using steady-state equations in the phasor-domain as

$$\vec{i}_{diff,ac} = -\frac{\vec{v}_{diff,ac}}{jX_L} \quad (28)$$

$$\vec{i}_{s,ac} = -\frac{\vec{v}_{s,ac}}{jX_{eq}} \quad (29)$$

Where X_L and X_{eq} denote the reactances of L and L_{eq}. (28) and (29) are derived by keeping only ac components in (14) and (15) and taking them to the phasor-domain. (28) and (29) can be reformulated in the time-domain by replacing (26) and (27) as

$$i_{diff,ac}(t) = \frac{-v_{ac}}{X_L}\cos\left(\frac{\varphi}{2}\right).\cos\left(wt+\frac{\varphi}{2}-\frac{\pi}{2}\right) \quad (30)$$

$$i_{s,ac}(t) = \frac{v_{ac}}{X_{eq}}\sin\left(\frac{\varphi}{2}\right).\cos\left(wt+\frac{\varphi}{2}\right) \quad (31)$$

The dc part of p^{Σ} and p^{Δ} are the average powers, p^{Σ} and P^{Δ}, and can be calculated by

$$\frac{dw_{DC}^{\Delta}}{dt} = P^{\Delta} = v_{diff,dc}.i_{s,dc} + 2v_{s,dc}.i_{diff,dc} + \langle v_{diff,ac}.i_{s,ac}\rangle_{T_{sw}} + \langle 2v_{s,ac}.i_{diff,ac}\rangle_{T_{sw}} \quad (32)$$

$$\frac{dw_{DC}^{\Sigma}}{dt} = p^{\Sigma} = 2v_{diff,dc}.i_{diff,dc} + v_{s,dc}.i_{s,dc} + \langle 2v_{diff,ac}.i_{diff,ac}\rangle_{T_{sw}} + \langle v_{s,ac}.i_{s,ac}\rangle_{T_{sw}} \quad (33)$$

where w_{DC}^{Δ} and w_{DC}^{Σ} are the dc parts of the differential and the sum energies and $\langle g\rangle_{T_{sw}}$ exhibits the average value of g over T_{sw} which is the switching period ($T_{sw}=\frac{1}{f}$). Using (26), (27), (30) and (31), $\langle v_{diff,ac}.i_{s,ac}\rangle_{T_{sw}}$ and $\langle 2v_{s,ac}.i_{diff,ac}\rangle_{T_{sw}}$ are found as

$$\langle 2v_{s,ac}.i_{diff,ac}\rangle_{T_{sw}} = \frac{v^2{}_{ac}}{2X_L}\sin(\varphi) \quad (34)$$

$$\langle v_{diff,ac}.i_{s,ac}\rangle_{T_{sw}} = \frac{v^2{}_{ac}}{4X_{eq}}\sin(\varphi) \quad (35)$$

From (30) and (31), it can be understood that between $v_{diff,ac}$ and $i_{diff,ac}$, and $v_{s,ac}$ and $i_{s,ac}$, there exists a 90-degree phase difference. Therefore, $\langle 2v_{diff,ac}.i_{diff,ac}\rangle_{T_{sw}}$ and $\langle v_{s,ac}.i_{s,ac}\rangle_{T_{sw}}$ are equal to zero. In the end, (24) and (25) are rewritten as

$$\frac{dw_{DC}^{\Delta}}{dt} = P^{\Delta} = v_{diff,dc}.i_{s,dc} + 2v_{s,dc}.i_{diff,dc} + \frac{v^2{}_{ac}}{4}\sin(\varphi)\left(\frac{1}{X_{eq}}+\frac{2}{X_L}\right) \quad (36)$$

$$\frac{dw_{DC}^{\Sigma}}{dt} = p^{\Sigma} = 2v_{diff,dc}.i_{diff,dc} + v_{s,dc}.i_{s,dc} \quad (37)$$

Using the Forward Euler equation, (36) and (37) can be discretized as presented in (38) and (39)

$$w_{DC}^{\Delta}(t+T_s) = w_{DC}^{\Delta}(t) + T_s.\left(v_{diff,dc}(t).i_{s,dc}(t) + 2v_{s,dc}(t).i_{diff,dc}(t) + \frac{v^2{}_{ac}(t)}{4}\sin(\varphi(t))\left(\frac{1}{X_{eq}}+\frac{2}{X_L}\right)\right) \quad (38)$$

$$w_{DC}^{\Sigma}(t+T_s) = w_{DC}^{\Sigma}(t) + T_s.(v_{s,dc}(t).i_{s,dc}(t) + 2v_{diff,dc}(t).i_{diff,dc}(t) \quad (39)$$

Equations (18), (19), (38), and (39) set up the discrete-time model of the dc/dc MMC.

IV. THE PROPOSED MPC METHOD FOR THE DC/DC MMC

From the developed discrete-time model, $i_{s,dc}$, $i_{diff,dc}$, w_{DC}^{Δ} and w_{DC}^{Σ} are the control objectives and $v_{s,dc}$, $v_{diff,dc}$ and φ are the control variables in the dc/dc MMC. To regulate each of them, first, the control set should be found based on the existing error. Then, the control set, which minimizes the defined cost function, is selected as the optimum state.

A. OUTPUT CURRENT

By looking at (19), it can be understood that the dc output current $i_{s,dc}(t+T_s)$ can be regulated by a proper value of dc output voltage $v_{s,dc}(t)$. In (19), V_{DC1} and V_{DC2} are constant values and the dc output current $i_{s,dc}(t)$ is measured from the circuit. At each time instant t, the control algorithm evaluates three different values of $v_{s,dc}$ including the current state $v_{s,dc}(t-T_s)$. The evaluated control set $V_{s,dc}(t)$ at time instant t is shown in (40).

$$V_{s,dc}(t) = \{v_{s,dc}(t-T_s) - \Delta v_{s,dc}(t), v_{s,dc}(t-T_s) \; v_{s,dc}(t-T_s) + \Delta v_{s,dc}(t)\} \quad (40)$$

where $\Delta v_{s,dc}(t)$ is the voltage step change at time instant t which is found by the control algorithm. Large values of $\Delta v_{s,dc}$ improve the dynamic performance, while small values enhance the steady-state performance. Therefore, an adaptive search step proposed in [25] is used. $\Delta v_{s,dc}(t)$ can be found in (41).

$$\Delta v_{s,dc}(t) = \begin{cases} v_{s,dc}^{up} & \gamma_s.E_s(t) > v_{s,dc}^{up} \\ \gamma_S.E_s(t) & v_{s,dc}^{up} > \gamma_S.E_S(t) > v_{s,dc}^{lw} \\ v_{s,dc}^{lw} & \gamma_S.E_S(t) < v_s^{lw} \end{cases} \quad (41)$$

where $v_{s,dc}^{up}$, $v_{s,dc}^{lw}$ are the upper and lower limits of $\Delta v_{s,dc}$, and γ_s is a constant which translates the dc output current error E_s into a meaningful output voltage. $E_s(t)$ is calculated by

$$E_s(t) = \frac{\left|i_{s,dc}(t) - i_{s,dc}^*\right|}{i_{s,dc}^*}, \; i_{s,dc}^* = \frac{P}{2V_{DC1}} \quad (42)$$

In (42), $i_{s,dc}^*$ is the dc output current reference of one phase-leg. $v_{s,dc}^{up}$, $v_{s,dc}^{lw}$ and γ_s are the design parameters which can be tuned to reach the desired steady-state and dynamic performances. Further explanation of the adaptive search step is not provided here, and it can be found in [25] and [29]. In this study, $v_{s,dc}^{up}$, $v_{s,dc}^{lw}$ and γ_s are selected as $0.1V_{DC2}$, $0.005V_{DC2}$ and $0.5V_{DC2}$.

To evaluate each control set, the following cost function $C_s(t)$ is designed.

$$C_s(t) = \left|i_{s,dc}(t+T_s) - i^*_{s,dc}\right| + \beta_s \left|v_{AC,max}(t+T_s) - v_{AC,ss}\right| \quad (43)$$

where β_s is a soft weighting factor. The first term regulates the dc component of output current. The second term improves the converter performance by maximizing the arm ac voltage during transient and steady states. Furthermore, it eliminates unnecessary changes in $v_{s,dc}$. Maximizing the arm ac voltage helps the controller to have better control over the differential energy, which will be discussed later. At each time instant t, $i_{s,dc}(t+T_s)$ is estimated by replacing each control set in (19). To find $v_{AC,max}(t+T_s)$, it is assumed that $v_{diff,dc}$ is equal to $\frac{V_{DC2}}{2}$, since from a control perspective, it should always be around $\frac{V_{DC2}}{2}$. The arms voltages, $v_{u,DC}$ and $v_{l,DC}$, are calculated using (10) and (11). Then $v_{AC,max}(t+T_s)$ is found from (5). For each control set, $C_s(t)$ is calculated, and the one minimizing the cost function is chosen. In this way, $v_{s,dc}(t)$ can be found.

B. DIFFERENTIAL CURRENT AND SUM ENERGY

From (18), it can be understood that by choosing a proper $v_{diff,dc}$, the dc component of differential current can be regulated. Similar to the control of output current, the control sets $V_{diff,dc}(t)$ are defined as

$$V_{diff,dc}(t) = \{v_{diff,dc}(t-T_s) - \Delta v_{diff,dc}(t), v_{diff,dc}(t-T_s), v_{diff,dc}(t-T_s) + \Delta v_{diff,dc}(t)\} \quad (44)$$

where $v_{diff,dc}(t-T_s)$ is the current state. $\Delta v_{diff,dc}(t)$ is the search step and can be found by (45).

$$\Delta v_{diff,dc}(t) = \begin{cases} \gamma_{diff}.E_{diff}(t) & \gamma_{diff}.E_{diff}(t) > v^{lw}_{s,dc} \\ v^{lw}_{diff} & \gamma_{diff}.E_{diff}(t) < v^{lw}_{s,dc} \end{cases} \quad (45)$$

where $v^{lw}_{diff,dc}$ is the lower limit of $\Delta v_{diff,dc}$, and γ_{diff} is a constant. As shown, unlike the control of output current, in the control of differential current, large steps are voided ($v^{up}_{diff,dc}$ is eliminated). Since the inductance path of the differential current (L) is very small, even a small deviation of $v_{diff,dc}$ from $\frac{V_{DC2}}{2}$ is enough to regulate $i_{diff,dc}$. In this study, $v^{lw}_{s,dc}$ and γ_s are selected as $10^{-5}V_{DC2}$ and $10^{-4}V_{DC2}$. $E_{diff}(t)$ is calculated in (46).

$$E_{diff}(t) = \frac{\left|i_{diff,dc}(t) - i^*_{diff,dc}(t)\right|}{i^*_{diff,dc}} \quad (46)$$

In which $i^*_{diff,dc}$ is the differential current reference.

To evaluate each control set, the following cost function is defined.

$$C_{diff}(t) = \left|i_{diff,dc}(t+T_s) - i^*_{diff,dc}(t+T_s)\right| \quad (47)$$

At each time instant t, $i_{diff,dc}(t+T_s)$ is estimated for each control set using (18). The differential current reference in the next sampling period $i^*_{diff,dc}(t+T_s)$ can be defined so that the sum energy can be regulated. In this regard, (39) is written at time instant $t+T_s$ and $i_{diff,dc}(t+T_s)$ is formulated as shown in (48).

$$i_{diff,dc}(t+T_s) = \left(\frac{1}{2v_{diff,dc}(t+T_s)}\right)\left(\frac{w^{\sum}_{DC}(t+T_s) - w^{\sum}_{DC}(t+2T_s)}{T_s} + v_{s,dc}(t+T_s).i_{s,dc}(t+T_s)\right) \quad (48)$$

Since the control of sum energy should be slow, the dynamics of $v_{diff,dc}$ and $v_{s,dc}$ can be ignored. As a result, instead of $v_{diff,dc}(t+T_s)$ and $v_{s,dc}(t+T_s)$, the steady-state values, $\frac{V_{DC2}}{2}$ and $\frac{V_{DC2}}{2} - V_{DC1}$, are replaced in (48). $i_{s,dc}(t+T_s)$ is estimated by replacing the obtained $v_{s,dc}(t)$ in the previous stage in (19). $w^{\sum}_{DC}(t+T_s)$ is also estimated by replacing the steady-state values of $v_{diff,dc}(t)$ and $v_{s,dc}(t)$ and the measured values of $i_{s,dc}(t)$ and $i_{diff,dc}(t)$ in (39). $w^{\sum}_{DC}(t+2T_s)$ needs to be replaced with the reference value of $w^{\sum}_{DC}$ at time instant $t+2T_s$. To find it, $w^{\sum}_{DC}(t+2T_s)$ can be formulated as

$$w^{\sum}_{DC}(t+2T_s) = \frac{T_s}{T_{sw}}\left(\sum_{k=0}^{\frac{T_{sw}}{T_s}-1} W^{\sum}(t+2T_s-kT_s)\right) = \frac{T_s}{T_{sw}}\left(\sum_{k=1}^{\frac{T_{sw}}{T_s}-1} W^{\sum}(t+2T_s-kT_s) + W^{\sum}(t+2T_s)\right) \quad (49)$$

As demonstrated in (49), $w^{\sum}_{DC}(t+2T_s)$ is split into two parts. The first part is the summation of $W^{\sum}$ from the time instant $t+3T_s-T_{sw}$ to $t+T_s$. This term can be calculated using the estimated average sum energy $w^{\sum}_{DC}(t+T_s)$ as

$$\sum_{k=1}^{\frac{T_{sw}}{T_s}-1} W^{\sum}(t+2T_s-kT_s) = \left(\frac{T_{sw}}{T_s}-1\right).w^{\sum}_{DC}(t+T_s) \quad (50)$$

Equation (50) is derived using the fact that between time instants $t+3T_s-T_{sw}$ and $t+T_s$ the average sum of energy is $w^{\sum}_{DC}(t+T_s)$. Instead of $W^{\sum}(t+2T_s)$, the reference value, which is equal to $Nc(\frac{V_{DC2}}{N})^2$ is replaced. c shows the SM capacitance. In the end, the sum energy reference at time instant $t+2T_s$ is calculated by

$$w^{\sum}_{DC,ref}(t+2T_s) = \left(1-\frac{T_s}{T_{sw}}\right).w^{\sum}_{DC}(t) + \frac{T_s}{T_{sw}}Nc\left(\frac{V_{DC2}}{N}\right)^2 \quad (51)$$

The defined sum energy reference pushes the sum energy towards the reference value at time instants $t+2T_s$. In this

way, after some sampling period, the average sum energy will settle down on the reference value $Nc(\frac{V_{DC2}}{N})^2$. This method lets the sum energy slowly approaches the reference value and prevents harsh transient and instability issues caused by fast changes in $v_{diff,dc}$. At the end of this stage, the dc differential voltage at the time instant-t $v_{diff,dc}(t)$ is found. Having $v_{s,dc}(t)$ and $v_{diff,dc}(t)$, the dc component of each arm voltage can be obtained. Then, the maximum ac voltage is found by (5), and it is used as the arm ac voltage for this switching cycle.

C. DIFFERENTIAL ENERGY

By fixing the arm ac voltage at the maximum feasible value, the differential energy is regulated by the phase difference between the arms ac voltages. At each time instant, three different values of φ are evaluated. The control set $\Phi(t)$ is defined in (52).

$$\Phi(t) = \{\varphi(t-T_s) - \Delta\varphi(t),\ \varphi(t-T_s)\ \varphi(t-T_s) + \Delta\varphi(t)\} \tag{52}$$

In (52), $\varphi(t-T_s)$ is the current state. The search step $\Delta\varphi(t)$ is found based on the error of differential energy at time instant t. Since the process of finding $\Delta\varphi(t)$ is the same as output current, further explanation in this regard is avoided. In this study, $\varphi^{up}_{s,dc}$, $\varphi^{lw}_{s,dc}$ and γ_φ are selected as 0.1π, 0.001π and 0.1π.

To evaluate each control set, the following cost function is defined.

$$C_{w^\Delta}(t) = \left|w^\Delta_{DC}(t+T_s) - w^\Delta_{DC,ref}(t+T_s)\right| + \beta_{w^\Delta}\left|\widehat{i}_{diff,ac}(t+T_s)\right| \tag{53}$$

In (53), $w^\Delta_{DC,ref}(t+T_s)$ is the reference differential energy, and β_{w^Δ} is a soft weighting factor. $\widehat{i}_{diff,ac}(t+T_s)$ denotes the ac circulating current. The first term in (53) controls the differential energy, and the second term tries to minimize the circulating current in the transient mode and the steady-state. $w^\Delta_{DC}(t+T_s)$ is estimated for each control set using (38). From (30), $\widehat{i}_{diff,ac}(t+T_s)$ is derived as $\frac{v_{AC,max}}{X_L}\cos(\frac{\varphi(t)}{2})$, and it is calculated for each control set. $w^\Delta_{DC,ref}(t+T_s)$ can be obtained by expanding $w^\Delta_{DC}(t+T_s)$ as follows:

$$w^\Delta_{DC}(t+T_s) = \frac{T_s}{T_{sw}}\sum_{k=1}^{\frac{T_{sw}}{T_s}-1} W^\Delta(t+T_s-kT_s) = \frac{T_s}{T_{sw}}\left(\sum_{k=1}^{\frac{T_{sw}}{T_s}-1} W^\Delta(t+T_s-kT_s) + W^\Delta(t+T_s)\right) \tag{54}$$

The first term is calculated using the measured dc sum energy $w^\Sigma_{DC}(t)$ in (55). This equation is derived using the fact that between time instants t and $t+2T_s-T_{sw}$, the average differential energy is $w^\Delta_{DC}(t)$.

$$\sum_{k=1}^{\frac{T_{sw}}{T_s}-1} W^\Delta(t+T_s-kT_s) = \left(\frac{T_{sw}}{T_s}-1\right).w^\Delta_{DC}(t) \tag{55}$$

Instead of the second term in (54), the reference value of W^Δ is replaced, which is equal to zero. This is because, ideally, each arm should store an equal amount of energy. In the end, $w^\Delta_{DC,ref}(t+T_s)$ is formulated in (56).

$$w^\Delta_{DC,ref}(t+T_s) = \left(\frac{T_{sw}}{T_s}-1\right).w^\Delta_{DC}(t) \tag{56}$$

By calculating C_{w^Δ} for each control set, the optimum phase-difference $\varphi(t)$ which minimizes the cost function is chosen.

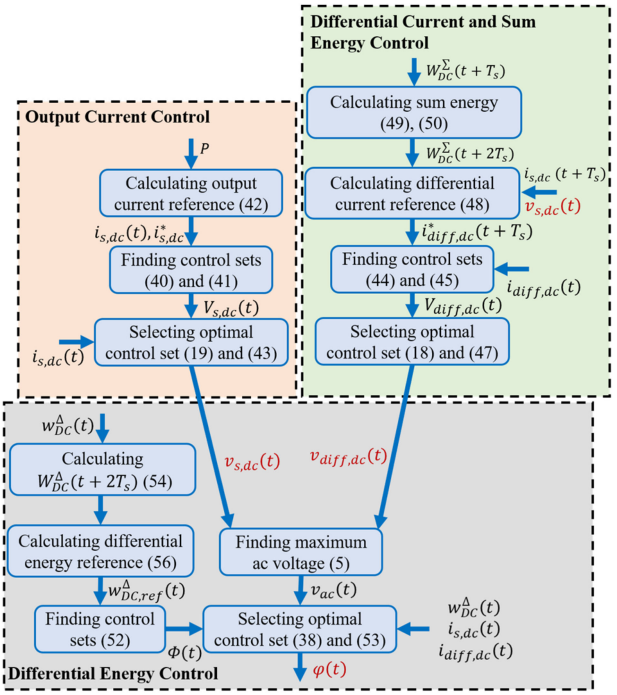

FIGURE 3. Overall flow chart of the proposed MPC of the dc/dc MMC.

D. OVERALL CONTROL DIAGRAM

As one can see in Fig. 3, the presented MPC approach for the dc/dc MMC has three parts, the dc output current, the dc differential current, and the dc differential energy. The first control stage is the output current regulation. Using the measured $i_{s,dc}(t)$, the search step of the output voltage is determined by (40), and then the control sets at time instant t are found by (41). The output current in the next sampling period $i_{s,dc}(t+T_s)$ is estimated by (19), and the cost function (43) is calculated for each of the control sets. The one minimizing the cost function is selected as the optimum output voltage $v_{s,dc}(t)$. In the control of dc differential current, the first task is to find the differential current reference $i_{diff,dc}(t+T_s)$ based on the sum energy using (48). The search step and control sets

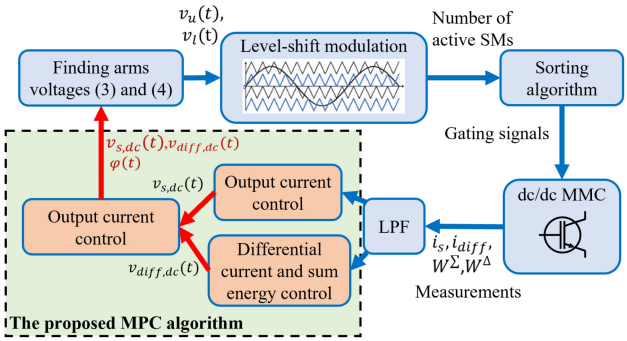

FIGURE 4. Overall control of the dc/dc MMC.

are calculated by (44) and (45). To find the optimum control set, the dc differential current in the next sampling period $i_{diff,dc}(t+T_s)$ is estimated by (18), and the cost function (47) is calculated for each control set. The one minimizing the cost function is selected as the optimum control set $v_{diff,dc}(t)$. After finding $v_{diff,dc}(t)$ and $v_{s,dc}(t)$, the maximum ac voltage $v_{AC,max}(t)$ is found using (5). At the same time, based on the measured dc component of differential energy, the control sets of phase-difference $\Phi(t)$ are found by (52). Finally, by estimating the differential energy by (38) and calculating the cost function (53), the optimum control set $\varphi(t)$ is determined.

In the end, the overall control diagram of the dc/dc MMC is demonstrated in Fig. 4. As shown, a low-pass filter with a bandwidth of 100 Hz is used to extract the dc component of measured variables. The proposed MPC method uses the dc variables to determine the control parameters $v_{s,dc}(t)$,$v_{diff,dc}(t)$ and $\varphi(t)$. Using (3) and (4), the arms voltages at time instant-t are calculated. Then, using the level-shift PWM technique, the number of active SMs at the next sampling period in each arm is found. Finally, using the sorting algorithm proposed in [30], the switched-on and -off SMs are determined based on the capacitors voltages of SMs.

E. TIME-DELAY COMPENSATION

So far, it is assumed that the system has no delay, and the calculated control voltages at time instant t can be applied instantaneously. However, in the real world, a time delay exists due to the A/D conversion delay, the calculation delay, and the zero-order-hold delay of the modulation process [31]. To account for the system delay, the calculated control voltages at time instant t must be applied at time instant $t+T_s$. The delay compensation is done using the method presented in [32]. An estimation step is added to the control algorithm, which is based on the known state of the system at time instant t, the system parameters are estimated at time instant $t+T_s$. Then based on the estimated parameters, the control voltages are calculated for the time interval between $t+T_s$ and $t+2T_s$. In this condition, the microprocessor have one sampling period T_s to calculate the control voltages.

TABLE 1. Calculation Time of the Basic Mathematical Operations

Mathematical Operation	Cycles
Sum\Subtraction	1
Multiplication	1
Comparison	1
Assignment	1
Absolute	2

TABLE 2. Comparison of Calculation Time

	Methods	Calculation Time
dc/ac MMC	Switching status based FCS-MPC [33]	$(5N+12).C_{2N}^{N}-1$
	Indirect FCS-MPC [34]	$161N^2+321N+160$
	Preselection based FCS-MMC [20]	$N^2+N+246$
	Modulated MPC based on the duty cycle [35]	$12N+160$
dc/dc MMC	Presented MPC method	$8N+169$

F. CALCULATION TIME CALCULATION

To assess the computional efficiency of the proposed MPC alogrithm, the calculation time of the MPC algorithm is found based on the calculation time of the basic mathematical operations. The number of cycles required for each mathematical operation is presented in Table I [25]. Using this Table, the calculation time of the proposed MPC algorithm is calculated. Because this paper proposes the first MPC approach for the control of the non-isolated dc/dc MMC, there are no other MPC methods to be compared with. Therefore, the calculation time of the proposed approach is compared with the methods developed for the control of the dc/ac MMC in Table II. As these two converters, the dc/dc MMC and the dc/ac MMC, share a lot of similarities (topology and control structure), this comparison can show how much the proposed MPC approach is computationally efficient. However, it is noteworthy that the operation principle, control objectives and the control variables are different in these two converters, which means the proposed MPC methods for the dc/ac MMC cannot be used directly for the dc/dc MMC. The presented calculation time is based on the number of SMs N and is calculated for one phase-leg. As can be seen, the proposed method has the lowest calculation time making it computationally efficient to be applied in large systems with hundreds of SMs.

V. SIMULATION STUDIES

Using detailed time-domain models to verify the research results in large-scale multilevel converters is a common and typical approach [10], [13]–[15], [18], [19], and it is used in this paper. To verify the effectiveness of the presented MPC approach, a dc/dc MMC with two phase-legs is simulated in

TABLE 3. Parameters of the Simulated DC/DC MMC

Common Parameter	Symbol	Value
Nominal Power	P	15 MW
DC-Link1 Nominal Voltage	V_{DC1}	14 kV
DC-Link2 Nominal Voltage	V_{DC2}	20 kV
Arm Inductor	L	1.2 mH
Phase Inductor	L_0	0.26 H
SM Capacitor	C	7 mF
SM Rated Voltage	V_{CN}	2 kV
AC Voltage Frequency	f	360 Hz
Number of Arm HBSMs	n	10
Sampling Frequency	$f_s\,(1/T_s)$	10 kHz
Weighting Factors	**Symbol**	**Value**
Output Current Cost Function	β_s	0.00001
Differential Energy Cost Function	$\beta_{w\Delta}$	0.1
PI Parameters	**Symbol**	**Value**
Proportionl Gain of Power Balance Controller	-	10
Integral Gain of Power Balance Controller	-	200
Proportionl Gain of DC-link Current Regulator	-	10
Integral Gain of DC-link Current Regulator	-	50

MATLAB\Simulink. The dc sides of the converter are connected to an ideal voltage source for the sake of simplicity. In the first case study, the steady-state performance of the presented MPC approach is investigated and compared with the results of the PI-based controller [16]. In the second case study, the transient performance of both the presented MPC approach and the conventional PI-based controller is compared. The converter parameters, and the control parameters of both the proposed MPC approach and the PI-based controller are exhibited in Table III. In the developed MPC method, the designed cost functions have only one weighting factor associated with the secondary term. To find the weighting factors, they are initially set to zero. Starting from zero, the weighting factors are increased to improve the converter performance. At some point, the regulation of the main control objective will be deteriorated because of the excessive increase of the weighting factor. Having this in mind, the soft weighting factors can be determined with try and error [36]. The optimum PI-controller parameters are found based on the process proposed in the original paper [16].

A. CASE STUDY I: STEADY-STATE

The results of the steady-state operation when the proposed MPC approach is employed are presented in Fig. 5. In this case, the converter transmits the nominal power (15 MW). The dc-links currents (i_{DC1} and i_{DC2}) and the output current of phase-leg 1 (i_{1o}) are exhibited in Fig. 5(a). As shown, a small amount of ac current is leaked from the phase-leg 1 (see the waveform of i_{1o}). However, because there exists a 180-degree phase difference between the output currents of the phase-legs 1 and 2, the leaked circulating currents from the phase legs

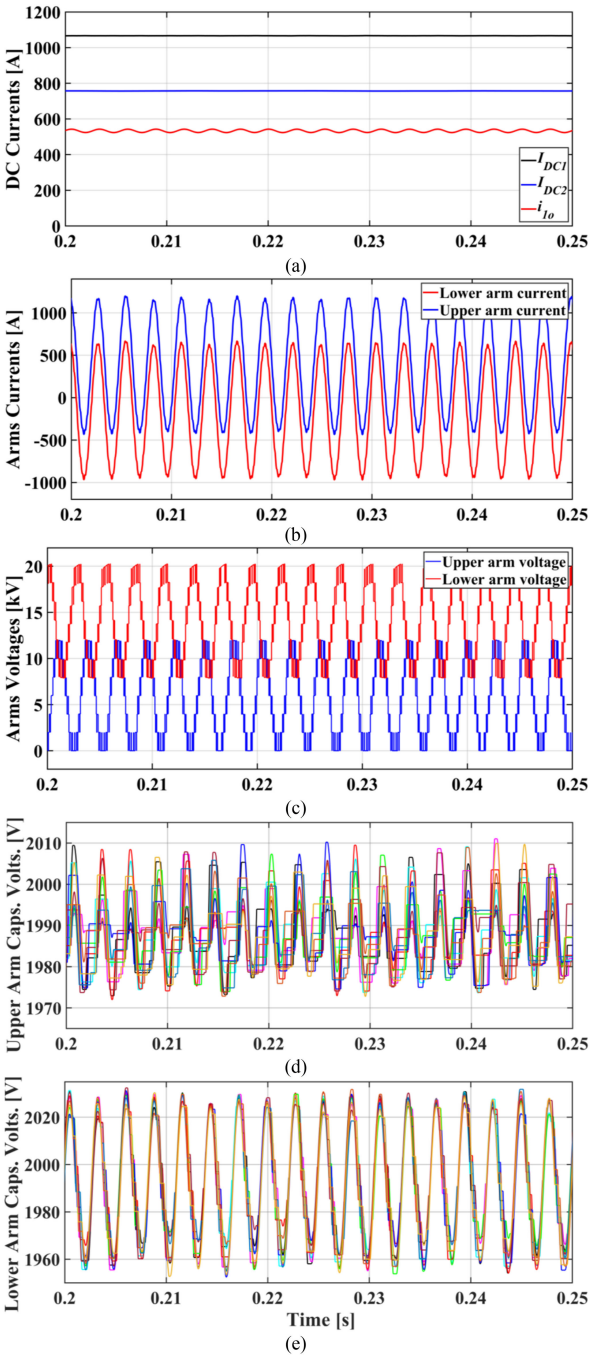

FIGURE 5. The steady-state operation of the proposed MPC approach, (a) the dc-links currents and the phase-leg 1 current, (b) the arms currents, (c) arms voltages, (d) the SMs voltages of the upper arm, (e) the SMs voltages of the lower arm.

canceled out each other at the conjunction point, providing very smooth dc currents in the dc-links. The arms currents are depicted in Fig. 5(b), which have dc and ac parts. The dc components of arms voltages regulate the dc part, enabling transmission of dc power. The ac part is generated by the arms ac voltages, and it intends to offset the exchanged dc power in the arms. Fig. 5(c) presents the arms voltages. As shown,

TABLE 4. Comparison of the PI Controller and the Presented MPC Approach in the Steady-State

Parameters	Conventional PI Controller	Proposed MPC
THD of I_{DC1} [%]	0.05	0.03
THD of I_{DC2} [%]	0.03	0.07
THD of i_{1o} [%]	1.76	1.78
Amplitude of Circulating Current [A]	796.5	717
Conduction Loss [kW]	50.5	47.3
Switching Frequency [Hz]	Upper arm: 650	Upper arm: 630
	Lower arm: 880	Lower arm: 857
Switching Loss [kW]	15.4	14.9
Total Loss [kW]	65.9	62.1

the lower arm has a higher dc voltage (14 kV), and this arm voltage varies from 8 kV to 20 kV in one fundamental period. The upper arm voltage changes from 0 to 12 kV. The dc part is equal to 6 kV. The amplitude of arm ac voltage is 6 kV, and this is the maximum possible value since the arms voltages are extended to the upper limit (20 kV) and the lower limit (0). The arms capacitors voltages are exhibited in Fig. 5(d) and (e). The SMs voltages of the lower arm fluctuate in a wider range compared to the SMs voltages of the upper arm. The results confirm the effectiveness of the presented MPC method in keeping the capacitors voltages balanced.

To compare the steady-state operation of the proposed MPC with the PI-based controller, Table IV is presented. In this Table, the switch loss characteristics are extracted from [37], and all the losses are calculated using the provided loss calculation model in MATLAB/Simulink [38] without considering the thermal effect. As can be seen, the THDs of dc-links 1 and 2 currents are very small for both approaches. The THD of the output current of phase-leg 1 for both methods are exhibited in Table IV, confirming that these two approaches have almost the same performance. The amplitude of the circulating current in the proposed MPC method is smaller than the PI-based controller (10 % smaller). It shows that the proposed MPC is more capable of reducing the ac circulating current. Accordingly, the conduction loss is calculated for both cases. As expected, the converter controlled by the proposed MPC approach has less conduction loss compared to the converter controlled by the PI controller, which is due to smaller ac circulating current. The switching frequency and switching losses are also calculated for both cases showing the fact that both approaches have almost the same switching losses. The obtained total loss confirms that the converter controlled by the proposed MPC approach operates more efficiently.

B. CASE STUDY II: TRANSIENT MODE PERFORMANCE

The main advantage of using the MPC method is the fast dynamic response. This scenario is designed to fully exhibit the proposed MPC approach's ability to respond to severe transient conditions. Initially, the converter transmits -15 MW. At t=0.3 s, the power reference of the converter changes to +15 MW. The simulation results of the presented MPC approach and the PI-based controller are illustrated in Figs. 6 and 7. The dc-links currents and the phase-leg 1 output currents are illustrated in Figs. 6(a) and 7(a). As shown, the proposed MPC approach offers a faster dynamic response compared to the PI-based controller. In the converter controlled by the PI controller, the dc-link 1 current and the phase-leg 1 currents reach the steady-state after 81 ms. While, in the converter controlled by the proposed MPC approach, they get to the steady-state in 60 ms. Similar observations are hold for the dc-link 2 current. As it reaches the steady-state in 120 and 85 ms in the PI controller and the proposed MPC approach, respectively. As can be seen, the proposed MPC approach improved the dynamic response more than 25 %. The improvement made in the dynamic response is not as expected from the MPC method. Because the external dynamic, i.e., the dc-links currents, heavily depends on the large phase-inductor. As a result, the dynamic response of dc-links currents is slow, and the MPC approach cannot further improve the dynamic response. The arms currents are presented in Figs. 6(b) and 7(b). The MPC method offers a smoother transient mode and a faster dynamic response. The arms voltages are presented in Figs. 6(c) and 7(c), where both methods show the same behavior in the transient phase. The SMs voltages are demonstrated in Fig. 6(d) and (e) and Fig. 7(d) and (e). As shown, in the proposed MPC approach, the dynamic response is much faster, and the overshoot of capacitors voltages is eliminated. This observation confirms that the presented MPC approach has better control over the sum and the differential energies compared to the PI-based controller.

C. CASE STUDY III: PARAMETRIC UNCERTAINTY

In the power system, designed components may have ±20% tolerance because of aging, temperature stresses, radiation, and distorted operation [39], [40]. Therefore, the proposed MPC approach for the dc/dc MMC should tolerate a degree of parametric uncertainty. By looking at the obtained discrete model of the dc/dc MMC, two system parameters, the arm inductance, and the phase inductance, can be found. Because the phase inductor is usually designed very large to filter the ac current, tolerance in this inductor is not impactful. However, variations in the arm inductance heavily influence the generation of the circulating current and the active ac power. Therefore, two different analyses are carried out to investigate the converter performance under parametric uncertainty. In the first one, the steady-state operation of the dc/dc MMC controlled by the proposed MPC approach is studied. In the second analysis, the transient response of both approaches,

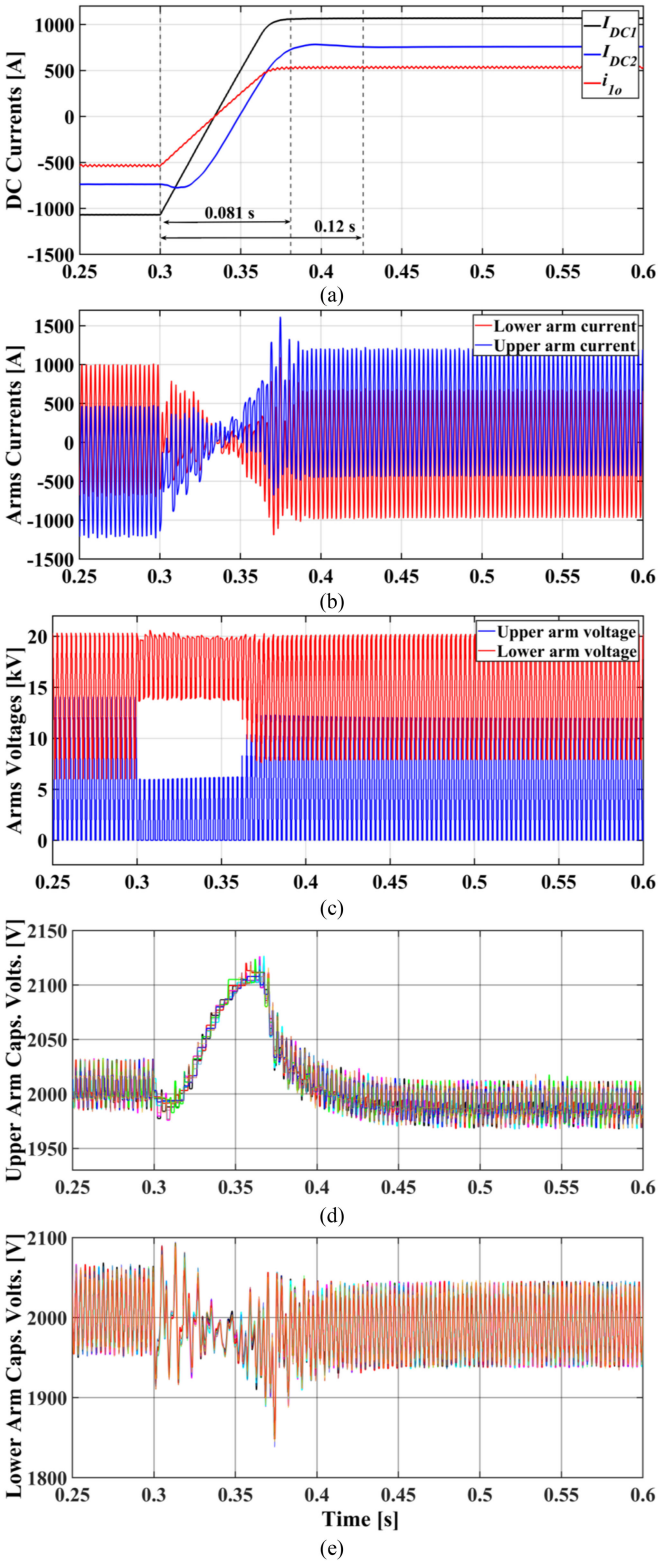

FIGURE 6. Conventional PI-based controller in transient mode, (a) the dc-links currents and the phase-leg 1 current, (b) the arms currents, (c) arms voltages, (d) the SMs voltages of the upper arm, (e) the SMs voltages of the lower arm.

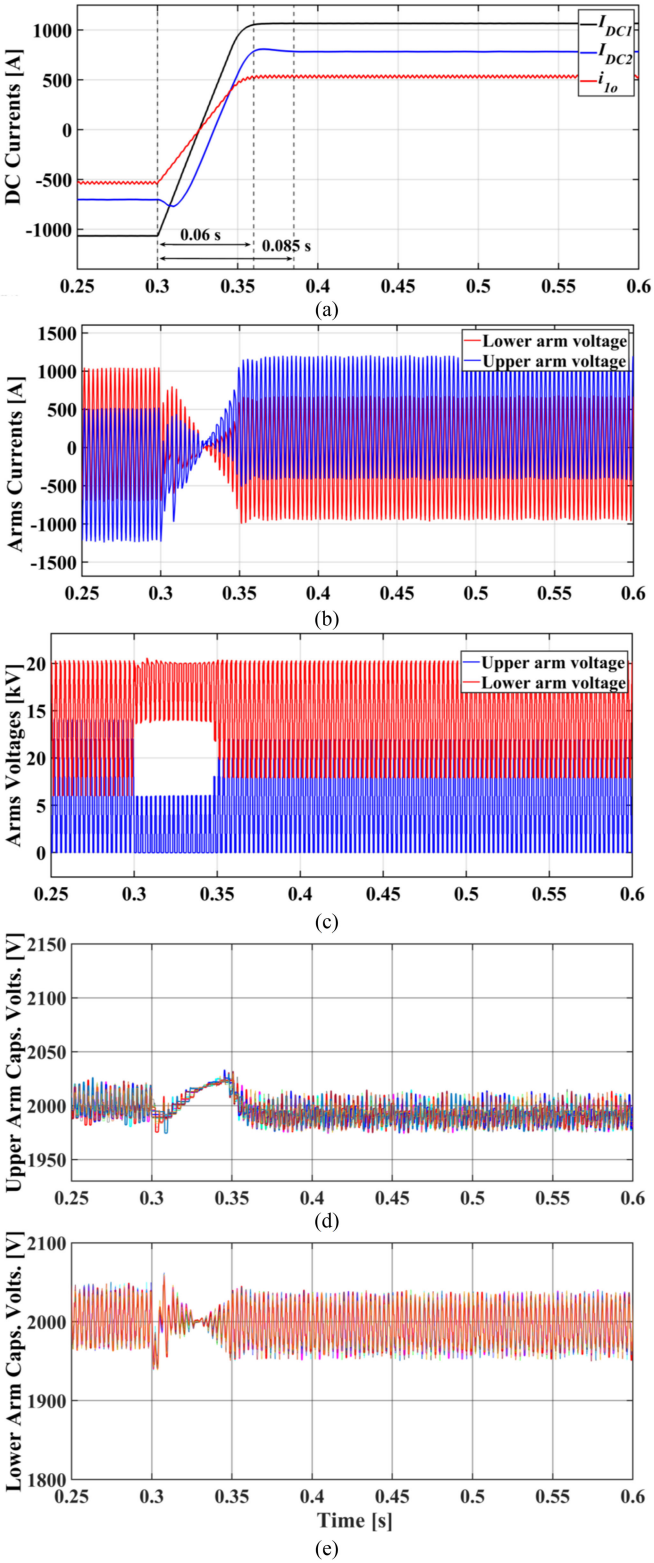

FIGURE 7. The proposed MPC approach in transient mode, (a) the dc-links currents and the phase-leg 1 current, (b) the arms currents, (c) arms voltages, (d) the SMs voltages of the upper arm, (e) the SMs voltages of the lower arm.

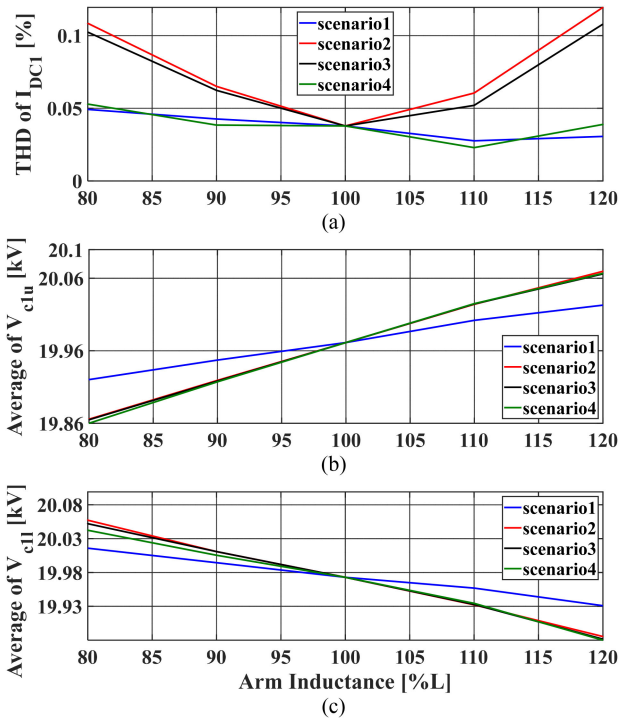

FIGURE 8. Sensitivity analysis, (a) THD of dc-link 1 current, (b) Average voltage of upper arm capacitors, (c) Average voltage of lower arm capacitors.

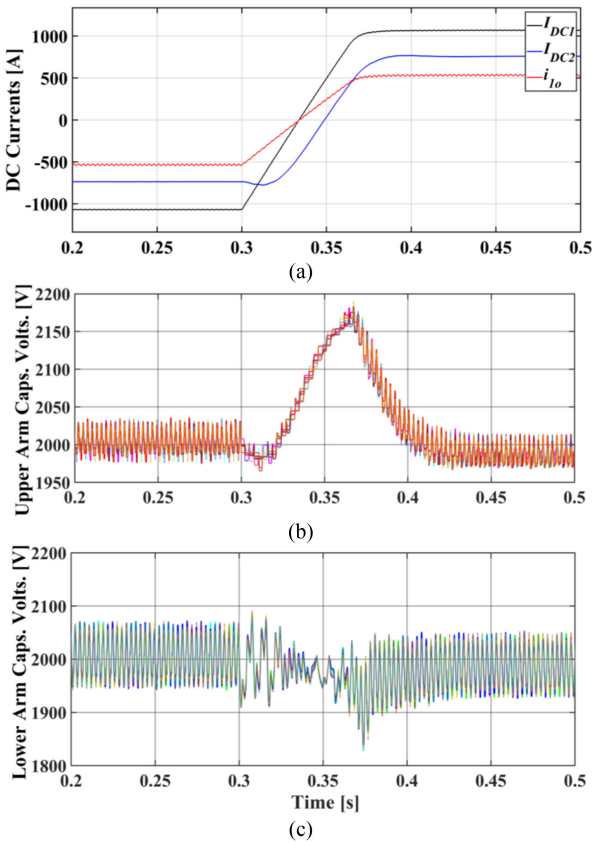

FIGURE 9. Conventional PI-based controller in transient mode under parametric uncertainty, (a) the dc-links currents and the phase-leg 1 current, (b) the SMs voltages of the upper arm, (c) the SMs voltages of the lower arm.

the PI controller and the proposed MPC, is compared when parametric uncertainty exists.

1) SENSITIVITY ANALYSIS

In this analysis, four different scenarios are assumed while the arm inductance changes between 80 % and 120% of the nominal value. The main purpose of defining these scenarios is to find the worst situation that the parametric uncertainty can happen. Scenario 1 is defined when the parametric uncertainty happens in one of the arm inductances in phase-leg 1. Scenario 2 refers to the situation in which both arms inductance in phase-leg 1 have uncertainty. In scenario 3, in addition to the arm inductances of phase-leg 1, one of the arm inductances in phase-leg 2 also varies between 80 % and 120% of the nominal value. In scenario 4, the parametric uncertainty occurs in all the arm inductances.

The results are illustrated in Fig. 8. The THD of dc-link 1 current is found for all the scenarios as the arm inductance varies between 80% and 120% of the nominal value in Fig. 8(a). Scenario 2 has the worst current THD in the whole range of arm inductance. Scenarios 1 and 4 have almost the same current THD, which is the lowest among the defined scenarios. As can be seen, even in the worst condition, the THD of dc-link 1 current is less than 0.2% showing the satisfactory performance of the proposed MPC approach despite parametric uncertainty. In Fig. 8(b) and (c), the average voltage of upper arm capacitors and lower arm capacitors are exhibited. As can be seen, scenario 1 is the closest to the reference voltage (20 kV); while the behaviors of scenarios 2, 3, and 4 are very similar. The change in the average capacitors voltages due to the parametric uncertainty is negligible, confirming that the proposed MPC approach is robust against the arm inductance variations.

2) TRANSIENT RESPONSE

The transient responses of the control methods, the PI controller, and the proposed MPC, while parametric uncertainty exists, are illustrated in Figs. 9 and 10. Initially, the converter transmits -15 MW. At t=0.3 s, the power reference of the converter changes to +15 MW. These simulation studies are carried out by considering that the arm inductances of the phase-leg 1 are 120% of the nominal value. As shown in Figs. 9(a) and 10(a), the parametric uncertainty does not impact the dc-links currents, and the response to the load transient is still faster in the converter controlled by the proposed MPC approach. The upper arm capacitors voltages are presented in Figs. 9(b) and 10(b). In the converter controlled by the PI controller, the transient response worsens compared to the case without the parametric uncertainty as the capacitors voltages reaches 2175 V in the transient period. Due to the parametric uncertainty, the average capacitors voltages of the

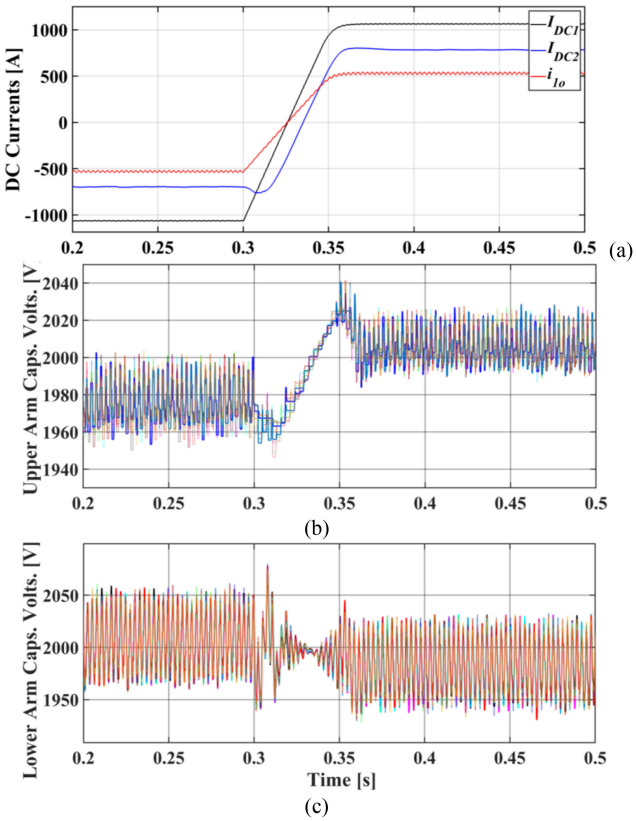

FIGURE 10. **The proposed MPC approach in transient mode under parametric uncertainty, (a) the dc-links currents and the phase-leg 1 current, (b) the SMs voltages of the upper arm, (c) the SMs voltages of the lower arm.**

upper arm is a little less than 2 kV before the load transient, and it is a little higher after the load transient. As shown in Figs. 9(c) and 10(c), the lower arm capacitors voltages are not impacted by the parametric uncertainty. In the end, it can be concluded that the performance of the converter controlled by the MPC approach is still superior despite of 20% variation in the arm inductance.

VI. CONCLUSION

This paper developed a Model Predictive Control (MPC) for the dc/dc Modular Multilevel Converter (MMC). First, the dynamic equations were extracted, and then, using the Forward Euler method, they were discretized. Using the discrete-time dynamic model of the converter, an MPC approach was developed to satisfy the control objectives by minimizing three separate cost functions. The simulation results of the presented MPC method and the conventional PI-based controller were compared in load transient and the steady-state. The advantages of the presented MPC approach are:

1) The internal dynamic, i.e., capacitors voltages and arms currents, and external dynamic, i.e., the injected currents into dc-links, are improved with the proposed MPC method is used.
2) The proposed MPC approach is more competent in reducing the circulating current in the steady-state. As a result, this improves the overall system efficiency.
3) Unlike the PI-based controllers with multiple parameters to be tuned, the proposed MPC approach offers a very straightforward implementation. Because the designed cost functions include one primary term and one secondary term with less importance, the tuning process of the weighting factors is very simple [36].

The robustness of the proposed MPC approach against parameter variation was investigated. The arm inductance was identified as the most effective element, where its variations impact the converter operation. The proposed approach can tolerate 20% tolerance in the arm inductance according to the obtained results.

REFERENCES

[1] G. J. Kish, "On the emerging class of non-isolated modular multilevel DC–DC converters for DC and hybrid AC–DC systems," *IEEE Trans. Smart Grid,* vol. 10, no. 2, pp. 1762–1771, Mar. 2019.
[2] G. P. Adam, I. A. Gowaid, S. J. Finney, D. Holliday, and B. W. Williams, "Review of dc–dc converters for multi-terminal HVDC transmission networks," *IET Power Electron.,* vol. 9, no. 2, pp. 281–296, 2016.
[3] J. D. Paez, D. Frey, J. Maneiro, S. Bacha, and P. Dworakowski, "Overview of DC–DC converters dedicated to HVdc grids," *IEEE Trans. Power Del.,* vol. 34, no. 1, pp. 119–128, Feb. 2019.
[4] S. Farzamkia, H. Iman-Eini, A. Khoshkbar-Sadigh, and M. Noushak, "A software-based fault-tolerant strategy for modular multilevel converter using DC bus voltage control," *IEEE J. Emerg. Sel. Topics Power Electron.*, vol. 9, no. 3, pp. 3436–3445, Jun. 2021, doi: 10.1109/JESTPE.2020.3022984.
[5] S. Farzamkia, M. Noushak, H. Iman-Eini, A. Khoshkbar-Sadigh, and S. Farhangi, "Fault-tolerant method to reduce voltage stress of submodules in postfault condition for regenerative MMC-based drive," *IEEE Trans. Ind. Electron.,* vol. 68, no. 6, pp. 4718–4726, Jun. 2021, doi: 10.1109/TIE.2020.2991998.
[6] S. Kenzelmann, A. Rufer, D. Dujic, F. Canales, and Y. R. d. Novaes, "Isolated DC/DC structure based on modular multilevel converter," *IEEE Trans. Power Electron.,* vol. 30, no. 1, pp. 89–98, Jan. 2015, doi: 10.1109/TPEL.2014.2305976.
[7] S. Norrga, L. Ängquist, and A. Antonopoulos, "The polyphase cascaded-cell DC/DC converter," in *Proc. IEEE Energy Convers. Congr. Expo.*, 2013, pp. 4082–4088.
[8] F. Zhang, G. Joós, and W. Li, "A transformer-less modular multilevel DC-DC converter with DC fault blocking capability," in *Proc. IEEE Southern Power Electron. Conf.*, Dec. 2017, pp. 1–6, doi: 10.1109/SPEC.2017.8333576.
[9] H. Yang, J. Qin, S. Debnath, and M. Saeedifard, "Phasor domain steady-state modeling and design of the DC–DC modular multilevel converter," *IEEE Trans. Power Del.,* vol. 31, no. 5, pp. 2054–2063, Oct. 2016, doi: 10.1109/TPWRD.2016.2515498.
[10] R. Razani and Y. Mohamed, "Augmented design of DC/DC modular multilevel converter improving efficiency and reducing number of SMs," *IEEE Trans. Power Del.,* vol. 35, no. 6, pp. 2905–2915, Dec. 2020, doi: 10.1109/TPWRD.2020.2991894.
[11] G. Kish and P. Lehn, "Linearized DC-MMC models for control design accounting for multi-frequency power transfer mechanisms," in *Proc. IEEE Power Energy Soc. Gen. Meeting*, Aug. 2018, pp. 1–1, doi: 10.1109/PESGM.2018.8586430.
[12] G. J. Kish and P. W. Lehn, "Modeling techniques for dynamic and steady-state analysis of modular multilevel DC/DC converters," *IEEE Trans. Power Del.,* vol. 31, no. 6, pp. 2502–2510, Dec. 2016, doi: 10.1109/TPWRD.2015.2508445.
[13] R. Razani and Y. A.-R. I. Mohamed, "Analysis of the unsymmetrical operation of the DC/DC MMC considering the DC-Link impedance," *IEEE Trans. Power Del.*, vol. 37, no. 3, pp. 1723–1733, Jun. 2022, doi: 10.1109/TPWRD.2021.3096498.

[14] R. Razani and Y. A. I. Mohamed, "Operation limits of the hybrid DC/DC modular multilevel converter for HVDC grids connections," *IEEE J. Emerg. Sel. Topics Power Electron.,* vol. 9, no. 4, pp. 4459–4469, Aug. 2021, doi: 10.1109/JESTPE.2020.3017206.
[15] R. Razani and Y. A. R. I. Mohamed, "Fault-tolerant operation of the DC/DC modular multilevel converter under submodule failure," *IEEE J. Emerg. Sel. Topics Power Electron.,* vol. 9, no. 5, pp. 6139–6151, Oct. 2021, doi: 10.1109/JESTPE.2021.3050122.
[16] H. Yang and M. Saeedifard, "A capacitor voltage balancing strategy with minimized AC circulating current for the DC–DC modular multilevel converter," *IEEE Trans. Ind. Electron.,* vol. 64, no. 2, pp. 956–965, Feb. 2017.
[17] H. Yang, M. Saeedifard, and A. Yazdani, "An enhanced closed-loop control strategy with capacitor voltage elevation for the DC–DC modular multilevel converter," *IEEE Trans. Ind. Electron.,* vol. 66, no. 3, pp. 2366–2375, Mar. 2019.
[18] F. Gruson, Y. Li, P. L. Moigne, P. Delarue, F. Colas, and X. Guillaud, "Full state regulation of the modular multilevel DC converter (M2DC) achieving minimization of circulating currents," *IEEE Trans. Power Del.,* vol. 35, no. 1, pp. 301–309, Feb. 2020, doi: 10.1109/TPWRD.2019.2942527.
[19] M. Cheah-Mane, J. Arevalo-Soler, E. Prieto-Araujo, and O. Gomis-Bellmunt, "Energy-Based control of a DC modular multilevel converter for HVDC grids," *IEEE Trans. Power Del.,* vol. 35, no. 4, pp. 1823–1833, Aug. 2020, doi: 10.1109/TPWRD.2019.2955007.
[20] B. Gutierrez and S. Kwak, "Modular multilevel converters (MMCs) controlled by model predictive control with reduced calculation burden," *IEEE Trans. Power Electron.,* vol. 33, no. 11, pp. 9176–9187, Nov. 2018, doi: 10.1109/TPEL.2018.2789455.
[21] X. Liu *et al.*, "A fast finite-level-state model predictive control strategy for sensorless modular multilevel converter," *IEEE J. Emerg. Sel. Topics Power Electron.,* vol. 9, no. 3, pp. 3570–3581, Jun. 2021, doi: 10.1109/JESTPE.2020.3008186.
[22] D. Zhou, P. Tu, H. Qiu, and Y. Tang, "Finite-Control-Set model predictive control of modular multilevel converters with cascaded open-circuit fault ride-through," *IEEE J. Emerg. Sel. Topics Power Electron.,* vol. 8, no. 3, pp. 2943–2953, Sep. 2020, doi: 10.1109/JESTPE.2019.2911959.
[23] J. Rodriguez-Bernuz and A. Junyent-Ferré, "Operating region extension of a modular multilevel converter using model predictive control: A single phase analysis," *IEEE Trans. Power Del.,* vol. 35, no. 1, pp. 171–182, Feb. 2020, doi: 10.1109/TPWRD.2019.2908695.
[24] J. Wang, X. Liu, Q. Xiao, D. Zhou, H. Qiu, and Y. Tang, "Modulated model predictive control for modular multilevel converters with easy implementation and enhanced steady-state performance," *IEEE Trans. Power Electron.,* vol. 35, no. 9, pp. 9107–9118, Sep. 2020, doi: 10.1109/TPEL.2020.2969688.
[25] Y. Jin *et al.*, "A novel sliding-discrete-control-set modulated model predictive control for modular multilevel converter," *IEEE Access,* vol. 9, pp. 10316–10327, 2021, doi: 10.1109/ACCESS.2021.3050340.
[26] B. Li, S. Shi, B. Wang, G. Wang, W. Wang, and D. Xu, "Fault diagnosis and tolerant control of single IGBT open-circuit failure in modular multilevel converters," *IEEE Trans. Power Electron.,* vol. 31, no. 4, pp. 3165–3176, Apr. 2016, doi: 10.1109/TPEL.2015.2454534.
[27] S. Martin and H. Li, "Model predictive control of an arm Inductor-less MMC-based DC SST," in *Proc. IEEE Appl. Power Electron. Conf. Expo.*, 2021, pp. 2113–2119, doi: 10.1109/APEC42165.2021.9487186.
[28] S. M. Akbar, A. Hasan, A. Watson, P. Wheeler, and S. Odhano, "Finite control set model predictive control of isolated DC/DC modular multilevel converter," in *Proc. IECON 46th Annu. Conf. IEEE Ind. Electron. Soc.*, 2020, pp. 5282–5289, doi: 10.1109/IECON43393.2020.9254434.
[29] Q. Xiao, L. Chen, H. Jia, P. W. Wheeler, and T. Dragičević, "Model predictive control for dual active bridge in naval DC microgrids supplying pulsed power loads featuring fast transition and online transformer current minimization," *IEEE Trans. Ind. Electron.,* vol. 67, no. 6, pp. 5197–5203, Jun. 2020, doi: 10.1109/TIE.2019.2934070.
[30] R. Razani, M. H. Ravanji, and M. Parniani, "Enhanced hybrid modular multilevel converter with improved reliability and performance characteristics," *IEEE Trans. Power Electron.,* vol. 34, no. 4, pp. 3139–3149, Apr. 2019, doi: 10.1109/TPEL.2018.2853625.
[31] J. Wang, Y. Tang, P. Lin, X. Liu, and J. Pou, "Deadbeat predictive current control for modular multilevel converters with enhanced steady-state performance and stability," *IEEE Trans. Power Electron.,* vol. 35, no. 7, pp. 6878–6894, Jul. 2020, doi: 10.1109/TPEL.2019.2955485.
[32] P. Cortes, J. Rodriguez, C. Silva, and A. Flores, "Delay compensation in model predictive current control of a three-phase inverter," *IEEE Trans. Ind. Electron.,* vol. 59, no. 2, pp. 1323–1325, Feb. 2012, doi: 10.1109/TIE.2011.2157284.
[33] J. Qin and M. Saeedifard, "Predictive control of a modular multilevel converter for a Back-to-Back HVDC system," *IEEE Trans. Power Del.,* vol. 27, no. 3, pp. 1538–1547, Jul. 2012, doi: 10.1109/TPWRD.2012.2191577.
[34] M. Vatani, B. Bahrani, M. Saeedifard, and M. Hovd, "Indirect finite control set model predictive control of modular multilevel converters," *IEEE Trans. Smart Grid,* vol. 6, no. 3, pp. 1520–1529, May 2015, doi: 10.1109/TSG.2014.2377112.
[35] D. Zhou, S. Yang, and Y. Tang, "Model-predictive current control of modular multilevel converters with phase-shifted pulsewidth modulation," *IEEE Trans. Ind. Electron.,* vol. 66, no. 6, pp. 4368–4378, Jun. 2019, doi: 10.1109/TIE.2018.2863181.
[36] P. Cortes *et al.*, "Guidelines for weighting factors design in model predictive control of power converters and drives," in *Proc. IEEE Int. Conf. Ind. Technol.*, Feb. 2009, pp. 1–7, doi: 10.1109/ICIT.2009.4939742.
[37] HiPak IGBT Module 5SNA 1500E250300. [Online]. Available: www.abb.com/semiconductors
[38] "Loss calculation in a three-phase 3-Level inverter." [Online]. Available: https://www.mathworks.com/help/physmod/sps/examples/loss-calculation-in-a-three-phase-3-level-inverter.html
[39] W. M. Smith, "Worst case circuit analysis-an overview (electronic parts/circuits tolerance analysis)," in *Proc. Annu. Rel. Maintainability Symp.*, 1996, pp. 326–334.
[40] N. Femia and G. Spagnuolo, "True worst-case circuit tolerance analysis using genetic algorithms and affine arithmetic," *IEEE Trans. Circuits Syst. I: Fundam. Theory Appl.,* vol. 47, no. 9, pp. 1285–1296, Sep. 2000.

RAMIN RAZANI received the B.Sc. degree in electrical engineering from the Isfahan University of Technology, Isfahan, Iran, in 2015, and the M.Sc. degree in electrical power engineering from the Sharif University of Technology, Tehran, Iran, in 2017. He is currently working toward the Ph.D. degree with the University of Alberta, Edmonton, AB, Canada. His research interests include modeling, control, and efficient design of multilevel converters with a special focus on HVDC systems.

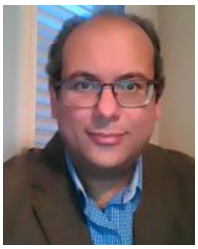

YASSER ABDEL-RADY I. MOHAMED (Fellow, IEEE) was born in Cairo, Egypt, on November 25, 1977. He received the B.Sc. (with Hons.) and M.Sc. degrees in electrical engineering from Ain Shams University, Cairo, Egypt, in 2000 and 2004, respectively, and the Ph.D. degree in electrical engineering from the University of Waterloo, Waterloo, ON, Canada, in 2008. He is currently a Professor with the Department of Electrical and Computer Engineering, University of Alberta, Edmonton, AB, Canada. His research interests include dynamics and controls of power converters, grid integration of distributed generation and renewable resources, microgrids, modeling, analysis, and control of smart grids, and electric machines and motor drives. Dr. Mohamed is an Associate Editor for IEEE TRANSACTIONS ON POWER ELECTRONICS, and the Editor of IEEE TRANSACTIONS ON POWER SYSTEMS, IEEE TRANSACTIONS ON SMART GRID, and IEEE POWER ENGINEERING LETTERS. He is a registered Professional Engineer in the Province of Alberta.